On the electrical and photoelectrical properties of CH3NH3PBI3 perovskites thin films

Mihaela Girtan

ON THE ELECTRICAL AND PHOTOELECTRICAL PROPERTIES OF $CH_3NH_3PbI_3$ PEROVSKITES THIN FILMS

Mihaela Girtan[1*]

[1]Photonics Laboratory, (LPhiA) E.A. 4464, SFR Matrix, Université d'Angers, Faculté des Sciences, 2 Bd Lavoisier, 49000 Angers, France

mihaela.girtan@univ-angers.fr

Keywords: $CH_3NH_3PbI_3$, perovskites, electrical conductivity, photoconductivity, time response, optical band gap

Abstract

Structural and morphological properties of $CH_3NH_3PbI_3$ thin films deposited by spin coating, with different spin speeds on glass and ITO patterned substrates were investigated. It results that long length acicular crystals, growth parallel to substrates (> 200µm for spin speeds of 800RPM/min). For low deposition spin speed these crystals are interconnected and deposited films present a high electrical conductivity. The XRD investigations indicate the formation generally of the cubic phase, or a mixture between cubic and tetragonal phase. For compact films the absorption is high over a large range of spectral domain (from 200 nm to 2100 nm), the transmission being lower than 20% in IR and less than 15 % in the visible domain. From electrical properties point of view, films are highly sensitive to light. An increase of the electrical conductivity with three order of magnitude is noticed when films are exposed to a white light of a solar simulator with an intensity of 1000W/m^2, but also an important increase is observed when films are exposed to a continuous low intensity ambient light, at least one order of magnitude in less than six seconds. This behavior is identical no matter the films thickness. The variation of the electrical conductivity at exposure to light in function of time and light intensity and the variation of the electrical conductivity in function of temperature were investigated and interpreted. The experimental results, since now, comforting the assumption of a multiband model.

Introduction

Last 5-6 years, a continuous growing interest was ascribed to hybrid organometallic halide perovskites due to their high potential application as materials for fourth generation solar cells [1]–[7]. Even if these materials are known since the 90s [8], [9] many of their properties and behavior are not completely understood. Since 2012, when a first solar cells using Methyl ammonium lead iodide ($CH_3NH_3PbI_3$) demonstrate its high efficiency to convert light, these cells are intensively studied and the attention is mainly focused on the whole device behavior and less on the material itself [10]. The high efficiency of solar cells using this perovskite material is attributed in general to the high absorption coefficient [11]. But this is not the only criteria which is important in the device functioning. The electrical conductivity and photoconductivity are key parameters for the development of efficient solar cells [7]. In order to bring a deeper understanding on the properties of perovskite thin films, in this paper the electrical conductivity and photoelectrical conductivity properties of $CH_3NH_3PbI_3$ thin films with different thickness deposited by spin coating are presented in correlation with their structural, morphological and optical properties.

Experimental

The precursor $CH_3NH_3PbI_3$ perovskite solution, was prepared using the proportions CH_3NH_3I:PbI_2:solvent as described in [12]. CH_3NH_3I (MAI) was purchased from Dyenamo and PbI_2 was purchased from Sigma-Aldrich. Each component was dissolved in a 1ml of a solution containing 0.8ml dry DMF and 0.2 ml DMSO and stirred at 60°C during two hours. Then, the two solutions containing the MAI and PbI_2 respectively, were mixed and stirred again during 30 min and then spin coated with different speeds on glass and ITO patterned substrates in identical conditions. The deposition parameters are given in Table I. Immediately after spin coating deposition, films were placed on a hot plate at 100°C and annealed for 45 min. Thin films thickness measurements were performed by profilometry and ellipsometry, using a Veeco Dektak 6M Stylus Profilometer and a Horiba Jobin Yvon ellipsometer respectively.

Films surface morphology was determined by Atomic Force Microscopy (AFM) with a Thermo-microscope VEECO and by Scanning Electron Microscopy (SEM) and by back scattered electron detection (BSD) with a Zeiss EVO LS10 Microscope. The structural characterization was made with a Cu-Kα (λ=1.5406Å) Bruker D8 Advance Diffractometer. The transmittance spectra were recorded in the wavelength range 280-1100nm with unpolarized light, at room temperature, using a Lambda 19 UV-Vis spectrophotometer.

Films deposited on ITO patterned substrates were used for perovskite thin films electrical measurements. To avoid the wettability problems, the substrates were subjected to a UV ozone

cleaner treatment during 15 min prior to the deposition. The configuration used for electrical and photoelectrical properties measurements is given in Fig.1. The distance between electrodes was of 1.5mm. The electrical resistance was measured using a source-meter Keithley 2400. The temperature dependence of the electrical conductivity has been studied in a temperature range 300K-383K in dark and under different illumination conditions.

Results and discussions

Perovskite films were deposited by using different spin speeds in order to analyze the influence of deposition parameters on the thin films properties. The highest rotation speed of 5000 RPM correspond to the usual deposition speed used for the preparation of perovskites thin films in solar cells [13]. The thinnest samples are noted with P0 and the thickest with P2. Films were deposited in identical conditions both on glass and ITO patterned substrates. For the studies of the perovskite thin films electrical properties, the active area is defined in-between the two ITO electrodes.

From the analysis of the surface morphology by scanning electron microscopy and chemical topography imaging (Fig.2), one can clearly remark the formation of acicular crystals and the percolation path for charge carriers between crystallites, for films deposited at lower speeds. The length of crystals increase with the decrease of rotation speed from about 50μm for 5000 RPM (sample P0) to about 150μm for 1500 RPM (sample P1) and 500μm for 800 RPM (sample P2). The crystallite size is important because can influences the transport of charge carriers. A better crystallization and large crystalline size are generally favorable to an improved transport of charge carriers. For lower deposition speeds (samples P1 and P2) the deposited films are compact and cover completely the ITO patterned substrates. For high spin speeds, crystals are small and there are not connected one to each other between the two electrodes (sample P0) and this explain why it wasn't possible to measure the electrical conductivity for sample P0.

The surface analysis was completed by structural XRD investigations. Previous studies showed that the methylammonium lead iodide ($MAPbI_3$) perovskite may exists in the cubic, tetragonal or orthorhombic phase [14]. The XRD spectra of the cubic and tetragonal phases are similar with slight differences that consist mainly from splitting of the peaks 100 and 200 of cubic phase to the 002, 110 and 004, 220 of the tetragonal phase, respectively. The most common criterion of XRD spectra to distinguish between them, is the presence of a peak at 23.68° in the XRD spectra which indicates the presence of the tetragonal 3D structure [15]. The peak at $2\theta = 14.29°$ can be deconvoluted into two peak components at 14.14° and 14.29° attributed to the 002 and 110 diffractions, respectively [1]. In our case, for the samples P0 and P1 the cubic phase is dominant. A

more pronounced evolution through the tetragonal phase is remarked for thicker films (Fig.3) sample P2. In this case we can remark the existence of the peaks of both phases: cubic and tetragonal. For all the samples, no peaks of PbI_2 at 12.3° are observed indicating that is no excess of PbI_2 and the reaction of perovskite formation was completed. From EDX analysis the atomic ratio between Pb and I was of 13.10% to 42.85%, which correspond to the expected ratio of 1:3, with a small excess of iodine.

The AFM analysis reveals the films perovskite surface morphology (Fig.4.). Here again the existence of the acicular crystal and their dimensions can be observed. The roughness is quite important and can be attributed to the height of crystals growth in acicular form, parallel to the substrate.

The transmission spectra for the $CH_3NH_3PbI_3$ films with different thickness deposited on glass substrates are given in Fig.5. For thickest films (sample P2) the transmission in the visible range is less than 15% and films exhibit also a high absorption in the near infrared range. For thinnest films the transmission is about 50% and this can be explained by the fact that the surface is not completely recovered as one can see from the SEM images of sample P0. The calculated absorption coefficient α values are of the order of 10^4 cm^{-1} (Fig. 6) and are in agreement with the values reported in literature [16]. A decrease of the values of α is remarked for photons with lower energy starting with 1.6 eV and lower. If the optical band gap is calculated from Tauc dependencies $(\alpha h\nu)^2$ vs. the photons energies $h\nu$, in the assumption of direct band transitions for semiconducting materials, as usual, the intercept of the linear part with the x-axis gives the value of the direct optical band gap of 1.56 eV. This value correspond to the experimental and calculated values obtained by other authors for, $CH_3NH_3PbI_3$ films [17], [18]. However, from the transmissions spectra, one can remark that the dependencies of transmission coefficient in function of wavelength do not correspond to the classical semiconductor behavior, for which a high transmission coefficient is generally observed (more than 80%) for high values of photons wavelength indicating the fact that photons with energies lower than the optical band gap energy cannot be absorbed. For $MAPbI_3$ thin films we can remark a decrease of the transmission coefficient with about only 10%-15 % between the region of lower absorption (1200 nm) and the region with higher absorption (300 nm). The measurements of transmission spectra on extend wavelength ranges 200nm-2200nm, (not shown here), conducted to the same conclusions. For example for the sample P2 the values of the transmission coefficient at 300 nm is of 15% and at 2200nm is of 32 % and for the sample P1 the transmission coefficient at 300 nm is of 25% and at 2200nm is of 35 %. The decrease of the transmission coefficient occurs in the same range for all the samples: between 790 and 750 nm. The small differences in the transmission coefficient can questioning the model of a semiconductor with one direct optical gap and the band gap calculations

from Tauc dependencies. From transmission spectra it results that photons with energies higher than 1.6 eV are highly absorbed, but also the photons from the IR part of the spectrum, with lower energies, are absorbed in a proportion of 30 to 50% in function of the thickness of the samples. The question that arise is: "the absorbed photon energy is transferred to valence band electrons or (and) to the free electrons of conduction band (absorption on free charges)?". The high efficiencies of solar cells based on $MAPbI_3$ thin films can be understand in part, on the basis of the high absorption coefficient values, but this absorption can be efficiently only if it generate a larger number of free charge carriers.

Hence, in order to progress in the understanding of $MAPbI_3$ thin films properties and their role in the high efficiencies and I-V hysteresis of solar cells, we also studied the response in time of the photoconductivity and temperature dependencies of conductivity and photoconductivity.

The electrical conductivity of samples P1 and P2 for films deposited with spin speed of 1500 RPM and 800 RPM respectively was measured between the two ITO electrodes, spaced with a distance of 1.5mm.in dark and under different illumination under the white light of a solar simulator.

The time response of the electrical photoconductivity was studied in two conditions. First the samples were kept in dark during more than 15 minutes and then were exposed to a very slight irradiation of $6W/m^2$, close to the usual ambient light working conditions. Second the samples kept under the ambient light conditions during more than 15 minutes were exposed to a white light irradiation of $180W/m^2$. The time responses of the electrical conductivity of the two samples are given in Figure 7. The results are very similar for the two samples indicating that this behavior do not depend on the samples thickness. The time response is of order of few seconds and the sensitivity of samples to light exposure is very high. The electrical conductivity increase quite fast at the exposure to light even for very low intensity levels of irradiation and then, after about 6 to 8 seconds, remains quite constant. The time response is of the same order of magnitude both at the exposure of sample from dark conditions to ambient light conditions or from ambient light conditions to $180W/m^2$ irradiation with a white light source. The time necessary to the system to recover after light exposure is much longer, for example, for an exposure of samples at 180 W/m^2 samples needs more than 20 s to attain a stabilized value of the electrical conductivity in dark conditions (Fig.8). The differences between the time response of the photoconductivity at the light exposure to light and the time that the system need, after the irradiation, to recover to initial state by recombination processes can explain, partly, the "hysteresis" observed in the I-V characterization of perovskite solar cells.

The electrical resistance decreases with at least of one order of magnitude even for very low levels of irradiation ($6W/m^2$) and with many orders of magnitude if samples are exposed to higher irradiation levels. For comparison, for a p-doped silicon sample (175μm thick) with similar dimension

at exposure to 180W/m^2 irradiation, the electrical resistance decreases from 9kΩ to 5 kΩ, in less than 100ms.

The dependencies of the electrical conductivity after attaining the stationary state, in function of the irradiation intensity are given in Figure 9. No significant differences were noticed, between the two samples having different thickness, this indicating a homogeneous polycrystalline structure and a behavior which is certainly specific to the material.

The photoconduction is the difference between the value of the electrical conductivity under irradiation and the value of the electrical conduction in dark. Hence, the photoconduction is strong correlated to the absorption processes and, in principle, there should be as many types of photoconduction as absorption processes are possible in semiconductors. Thus the simplest classifier is the one that establishes three types of photoconduction: intrinsic photoconduction, extrinsec photoconduction and the photoconduction on free charges carriers. Excepting the photoconduction on free charges, which suppose the modification of charge carrier mobilities, the intrinsic and extrinsic fotoconduction are related to an increase of number of electrons and holes in the conduction and valence band respectively. Due to the complexity of charges carriers generation and recombination mechanisms is difficult from mathematical point of view to establish a theoretical model which can be applied to all types of semiconductors. Is generally accepted that the intrinsic photoconduction is directly proportional to light intensity (Eq.1) for low irradiation intensities, and at high irradiation intensities the intrinsic photoconductivity is directly proportional to the square root of the light intensities (Eq.2) [19].

$$\Delta\sigma_{st} = e(\mu_n + \mu_p)\frac{\eta_\lambda \Phi(1-R)}{h\nu\, L_\lambda}\,\tau \qquad \text{Eq.1.}$$

$$\Delta\sigma_{st} = \left[e(\mu_n + \mu_p)\frac{\eta_\lambda \Phi(1-R)}{h\nu L_\lambda}\frac{\tau}{\gamma}\right]^{1/2}$$

Eq.2.

Here, e- is the elementary charge, μ_n and μ_p are the electron and holes mobilities, η_λ- is the quantum efficiency, R is the reflexion coefficient, Φ - is the light intensity γ - is the recombination coefficient, L_λ is the diffusion length, τ - is the relaxation time of electrons and $h\nu$ - the photon energy.

For extrinsic photoconduction $\Delta\sigma_{st}$ is direct proportional to Φ at low light intensity irradiations and tends towards a saturation value at high irradiation intensities.

By representing $\ln(\Delta\sigma_{st})$ in function of $\ln\Phi$ (inset of Fig.9), it is possible to identify these different ranges of photoconductivity variation. The slope of these curves calculated for the range comprise between 10 and 300 W/m^2 is around 0.5 indicating a square root dependence of $\Delta\sigma_{st}$ on Φ.

The square root dependence of electrical conductivity on light intensity was also noticed for $MAPbI_3$ films for measurements in a different configuration [20] on different mesoporous metal oxide scaffolds. This behavior was attributed to a band to band main generation-recombination mechanisms [20]. Despite the large crystal defects in perovskite films the dependencies of the photoconductivity on light intensity and temperature indicate that these defects do not introduce or the trap states do not influence significantly the transports mechanisms. For classical semiconductors a decrease of the resistivity with the increase of the temperature is generally observed and this is due to an increase of free charges carriers' concentration, by thermal activation. The measurements of the electrical conductivity done by A. Pisoni et all [21] on bulk material and by D. Głowienka et all [22] on thin films indicate different variation domains of the electrical conductivity and a metallicity and semiconducting electrical conductivity crossover in function of the temperature. This unusual behavior for a semiconductor, of the increase of the resistivity with the temperature increasing, was remarked for measurements in dark conditions by D. Głowienka [22] between 280K and 340K and under illumination measurements conditions by K. Sveinbjörnsson et al [20] between 293K and 353 K and by A. Pisoni et all [21] between 70K and about 140K and then between 150K and about 160K for low intensity light. Some authors attributed this behavior to a change transition between tetragonal to cubic phase, however is not clear if this transitions occurs both or not, under illumination and in dark. Moreover, if this crossover from non-metallic to metallic temperature dependence of the resistivity is due to a change phase transition, is not clear why the temperature range differs. The difficulties arises also from the limitations of instruments measurements range due to the very high values of resistivity of samples under dark measurements conditions (more than 200 GΩ), or due to the different range of measurements (below room temperature or up to the room temperature), ageing of samples etc. Our results, for measurements done between 27°C and 110°C (300K – 383K) under a white illumination of 70W/m2, are in agreement with the observations of K. Sveinbjörnsson et al [20]. The temperature range of this increase of the resistivity (decrease of conductivity), is also close to temperature range observed by D. Głowienka et all [22] for measurements in dark, who observed a decrease of the conductivity with three order of magnitude with the temperature increasing, from about $2x10^{-2}Sm^{-1}$ at about 300 K to $5x10^{-6}Sm^{-1}$ at 350K. In our case, the decrease of the electrical conductivity, under illumination, is small: from $2.5x10^{-2}Sm^{-1}$ at 300 K to from $2.5x10^{-2}Sm^{-1}$ at 380K. Slight variation, of same order of magnitude, were observed by K. Sveinbjörnsson et al [20] for samples prepared in different conditions and measured under illumination at $46W/m^2$ and $100\ W/m^2$. Figure 10 gives the variations of the electrical conductivity in function of temperature of two samples prepared in different conditions and having different thickness, the values of the electrical conductivity and the behavior in temperature for the measurements done under illumination with a white source and $70W/m^2$ conduct to identical results. That indicate that these

properties are intrinsic to the material, and the preparation conditions such as defaults, grain boundaries, thickness, influence little the general behavior of the $MAPbI_3$ spin coated films.

The electrical response in temperature, optical absorption and photoconductivity, suggest that model of band gaps for perovskite films could be different from that one of classical semiconductors. Indeed, is we analyze the theory of band gap for classical semiconductors, the displacement of electrons take place in a periodic potential with a 3D symmetry of barriers height in all the directions of the crystal. The calculations starting from the Schrodinger equation for the electron in a periodic potential in the Kroning-Penney model, conducted to the proof of the existence of the band gaps. The classification as metal or semiconductor or insulating material depend on the position of Fermi level and on the width of the band gap. The band gap diagram depend on the position of the atoms in crystals and the shape of the periodic potential. Different from classical semiconducting materials, one can remark that the shape of the periodic potential that an electron could see, when it traverse a $CH_3NH_3PbI_3$ crystal, depend on the direction on which the electron moves. Analyzing the specific structure of perovskite crystals (Fig.11) one can remark that the periodic potential created by the atoms positions can be different if function of the different trajectories that can be chosen for the displacement of the electrons through the crystal. The band gap diagrams, which can results for such type of crystal, could be seen as a results of the superposition of all possible combinations of these periodic potentials. Recent theoretical calculations of the band structure in $MAPbI_3$ [23] suggested a multiband model. In the classical approach band diagram models for semiconductors materials the band gap diagram correspond to the situation depicted in Fig.12a and Fig.12b in the assumption of direct and indirect transitions respectively. Fig. 12c corresponds to a semiconductor for which it exist an overlap of the balance and conduction band, that meaning that all energy levels are permitted. Fig.12.d is a proposed multiband model resulting from the overlapping or superposition of different periodic potentials such as could be the case of $MAPbI_3$ crystals. The experimental results, since now, comforting the assumption of a multiband model. In this assumption the high absorption over al large spectral domain can be explained first by the absorption of low energy photons, then when the lowest energy states were occupied, a second level of absorption is possible for photons with higher energies.

In the presence of continuous white light irradiation, lowest states are occupied and a lot of photo-generated free carriers are generated. The increase of resistivity with the temperature, when samples are measured under irradiation conditions, could be explained by the presence in the conduction band of an excessive high numbers of free carriers. This large number of free carriers, may lead to a decrease of the mobility (due to an increase of collisions between free charges), which, probably, is not compensated by the increase of the number of free charge carriers by thermal activation.

Conclusion

Structural and morphological properties of $CH_3NH_3PbI_3$ thin films deposited by spin coating in one step method from a solution containing MAI and PbI_2 dissolved in a mixture of DMF and DMSO. Films with different thickness were deposited on glass and ITO patterned substrates. It results that long length acicular crystals, growth parallel to substrates. For low deposition spin speed these crystals are interconnected and present high electrical conductivity. The XRD investigations indicate the formation of the cubic phase, or a mixture between cubic and tetragonal for thicker films. For compact films the absorption is high over the whole spectrum from UV to IR range, the transmission being lower than 20% in IR and less than 15 % in the visible domain. From electrical point of view, films are highly sensitive to light. An increase of the electrical conductivity with three order of magnitude is noticed when films are exposed to a white light irradiation of a solar simulator with an intensity of 1000W/m^2, but also an important decrease is also observed when films are exposed to a continuous low intensity ambient light, with a decrease of at least one order of magnitude in less than six seconds. This behavior is identical, no matter the films thickness. The variation of the electrical conductivity in function of time and light intensity and in function of temperature were investigated. From spectrophotometry data, electrical and photoelectrical behavior, a multiband model of the $MAPbI_3$ perovskite films seems to be more appropriate to describe the properties of this material.

Acknowledgements

The authors are grateful to Romain Mallet from SCIAM - Microscopy service for AFM and SEM micrographs and to Magali Alain and Nicolas Mercier from CRISTAL-MATRIX service platform for providing the necessary facilities for XRD studies.

Competing interests

The author declare no competing interests.

References

[1] A. Aukštuolis *et al.*, “Measurement of charge carrier mobility in perovskite nanowire films by photo-celiv method,” *Proceedings of the Romanian Academy Series A - Mathematics Physics Technical Sciences Information Science*, vol. 18, no. 1, pp. 34–41, 2017.

[2] J. Burschka *et al.*, “Sequential deposition as a route to high-performance perovskite-sensitized solar cells,” *Nature*, vol. 499, no. 7458, pp. 316–319, 2013.

[3] M. A. Green, A. Ho-Baillie, and H. J. Snaith, “The emergence of perovskite solar cells,” *Nature Photonics*, vol. 8, no. 7, pp. 506–514, 2014.

[4] H. J. Snaith *et al.*, “Anomalous hysteresis in perovskite solar cells,” *Journal of Physical Chemistry Letters*, vol. 5, no. 9, pp. 1511–1515, 2014.
[5] J. H. . Heo *et al.*, “Efficient inorganic-organic hybrid heterojunction solar cells containing perovskite compound and polymeric hole conductors,” *Nature Photonics*, vol. 7, no. 6, pp. 486–491, 2013.
[6] J. S. Shaikh *et al.*, “Perovskite solar cells: In pursuit of efficiency and stability,” *Materials and Design*, vol. 136, pp. 54–80, 2017.
[7] M. Girtan, “New trends in solar cells research,” *SpringerBriefs in Applied Sciences and Technology*, no. 9783319673363, pp. 45–75, 2018.
[8] N. Onoda-Yamamuro, T. Matsuo, and H. Suga, “Calorimetric and IR spectroscopic studies of phase transitions in methylammonium trihalogenoplumbates (II)†,” *Journal of Physics and Chemistry of Solids*, vol. 51, no. 12, pp. 1383–1395, 1990.
[9] N. Onoda-Yamamuro, O. Yamamuro, T. Matsuo, and H. Suga, “p-T phase relations of CH3NH3PbX3 (X = Cl, Br, I) crystals,” *Journal of Physics and Chemistry of Solids*, vol. 53, no. 2, pp. 277–281, 1992.
[10] R. Gottesman *et al.*, “Extremely slow photoconductivity response of CH3NH 3PbI3 perovskites suggesting structural changes under working conditions,” *Journal of Physical Chemistry Letters*, vol. 5, no. 15, pp. 2662–2669, 2014.
[11] M. A. Green, A. Ho-Baillie, and H. J. Snaith, “The emergence of perovskite solar cells,” *Nature Photonics*, vol. 8, no. 7, pp. 506–514, 2014.
[12] H.-S. Kim *et al.*, “Lead iodide perovskite sensitized all-solid-state submicron thin film mesoscopic solar cell with efficiency exceeding 9%,” *Scientific Reports*, vol. 2, 2012.
[13] F. Ebadi, N. Taghavinia, R. Mohammadpour, A. Hagfeldt, and W. Tress, “Origin of apparent light-enhanced and negative capacitance in perovskite solar cells,” *Nature Communications*, vol. 10, no. 1, p. 1574, Apr. 2019.
[14] S. Luo and W. A. Daoud, “Crystal structure formation of CH3NH3Pbi3-xClx perovskite,” *Materials*, vol. 9, no. 3, 2016.
[15] T. Baikie *et al.*, “Synthesis and crystal chemistry of the hybrid perovskite $CH_3NH_3PbI_3$ for solid-state sensitized solar cell applications,” *Journal of Materials Chemistry A*, vol. 1, no. 18, pp. 5628–5641, 2013.
[16] S. De Wolf *et al.*, “Organometallic halide perovskites: Sharp optical absorption edge and its relation to photovoltaic performance,” *Journal of Physical Chemistry Letters*, vol. 5, no. 6, pp. 1035–1039, 2014.
[17] E. Mosconi, A. Amat, M. K. Nazeeruddin, M. Grätzel, and F. De Angelis, “First-principles modeling of mixed halide organometal perovskites for photovoltaic applications,” *Journal of Physical Chemistry C*, vol. 117, no. 27, pp. 13902–13913, 2013.
[18] Y. Tu *et al.*, “Modulated CH3NH3 PbI3-x Brx film for efficient perovskite solar cells exceeding 18%,” *Scientific Reports*, vol. 7, 2017.
[19] G. M. Rusu and G. I. Rusu, *Bases of Semiconductors Phyiscs*, Editor “Al.I.Cuza” University, Iasi, 2015, Volume 4, page 189.
[20] K. Sveinbjörnsson *et al.*, “Probing Photocurrent Generation, Charge Transport, and Recombination Mechanisms in Mesostructured Hybrid Perovskite through Photoconductivity Measurements,” *Journal of Physical Chemistry Letters*, vol. 6, no. 21, pp. 4259–4264, 2015.
[21] A. Pisoni *et al.*, “Metallicity and conductivity crossover in white light illuminated CH3NH3PbI3 perovskite A.,” *arXiv:1604.05637 [cond-mat.str-el], 2016*.
[22] D. Głowienka, T. Miruszewski, and J. Szmytkowski, “The domination of ionic conductivity in tetragonal phase of the organometal halide perovskite CH3NH3PbI3-xClx,” *Solid State Sciences*, vol. 82, pp. 19–23, 2018.
[23] K. P. Ong *et al.*, “Multi Band Gap Electronic Structure in CH 3 NH 3 PbI 3,” *Scientific Reports*, vol. 9, no. 1, 2019.

Tables

Table I. Spin coating deposition parameters of perovskite thin films deposited on glass and ITO patterned glass substrates.

Sample	Spin deposition steps parameters	Thin films thickness (nm)
P0	5000 (RPM) 30 (s)	150-300
P1	1000/1500/1000 (RPM) 10/20/10 (s)	500-700
P2	600/800/600 (RPM) 10/20/10 (s)	1150-1580

FIGURE CAPTIONS

Figure-1. Electrical conductivity measurement configuration.

Figure-2. SEM micrographs chemical topography imaging by back scattered electron detection (BSD) for $CH_3NH_3PbI_3$ thin films deposited with different spin speeds on ITO patterned substrates (samples P0, P1 and P2).

Figure-3. XRD patterns for $CH_3NH_3PbI_3$ thin films deposited with different spin speeds on glass substrates.

Figure-4. 2D and 3D AFM images for $CH_3NH_3PbI_3$ thin films deposited with different spin speeds on glass substrates.

Figure-5. Transmission coefficients for $CH_3NH_3PbI_3$ thin films deposited with different spin speeds on glass substrates.

Figure-6. The absorption coefficient vs. photon energy for films $CH_3NH_3PbI_3$ thin films deposited on glass substrates with different rotations speeds

Figure-7. The variation of the electrical conductivity in function of time for the samples P1 and P2, after the exposure of the samples from dark conditions ($0W/m^2$) to ambient light ($6W/m^2$), and then from ambient light condition ($6W/m^2$) to an exposure under a white light source ($180W/m^2$).

Figure-8. The electrical conductivity variation in function of time after the irradiation with a white light source ($180W/m^2$), to ambient light conditions ($6W/m^2$).

Figure-9. The variation of the electrical conductivity in function of light intensity irradiation after the saturation regime is attaint (after more than 60 seconds) for two samples deposited with different spin speeds, having a different thickness. The inset gives the dependencies of the photoconductivity logarithm in function of the light intensity logarithm.

Figure-10. The variation of the electrical conductivity in function of temperature measured under illumination ($70W/m^2$) with a white light source during one cycle of heating and cooling for two samples deposited with different spin speeds, having a different thickness.

Figure-11. The unit cells for cubic, tetragonal and orthorhombic phases of $CH_3NH_3PbI_3$ perovskite.

Figure-12. Semiconductor band structures: a) aligned bands (direct band gap) b) not-aligned bands (indirect band gap) c) overlapped bands d) multiband model.

Figures

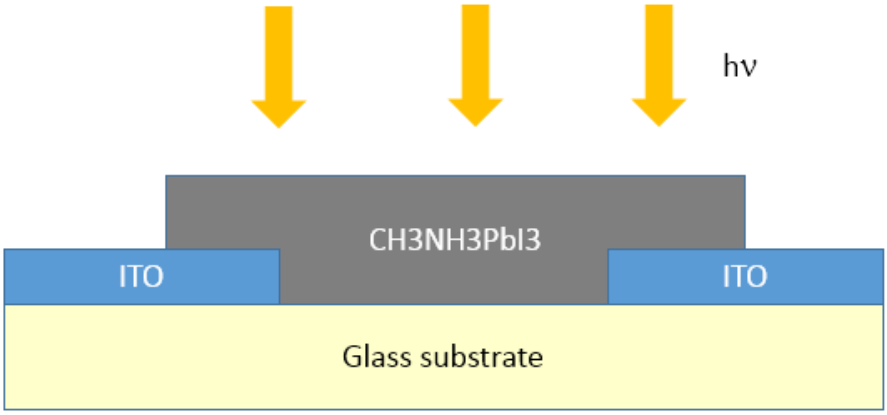

Figure-1. Electrical conductivity measurement configuration

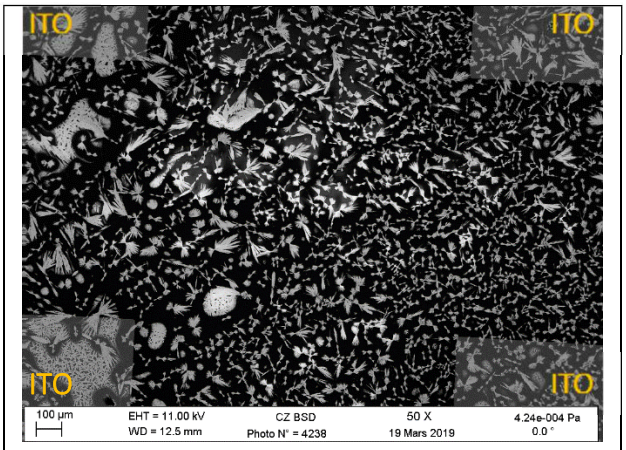

P0

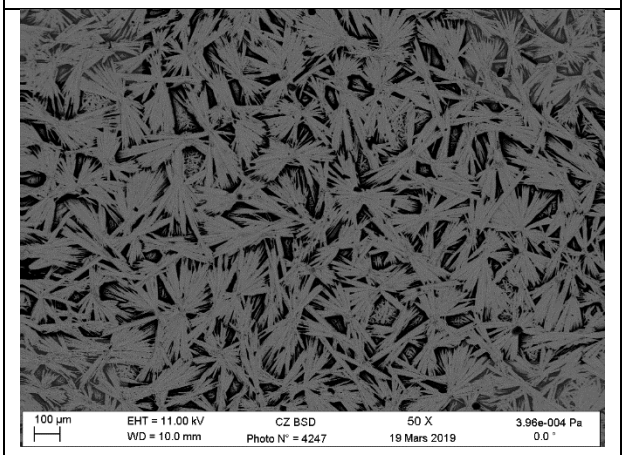

P1

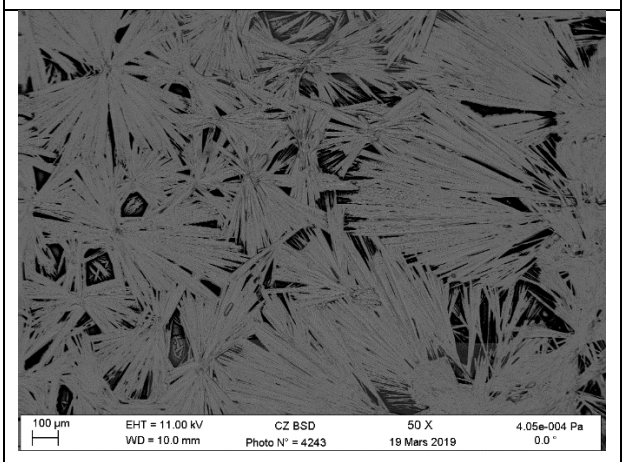

P2

Figure-2. SEM micrographs chemical topography imaging by back scattered electron detection (BSD) for $CH_3NH_3PbI_3$ thin films deposited with different spin speeds on ITO patterned substrates (samples P0, P1 and P2).

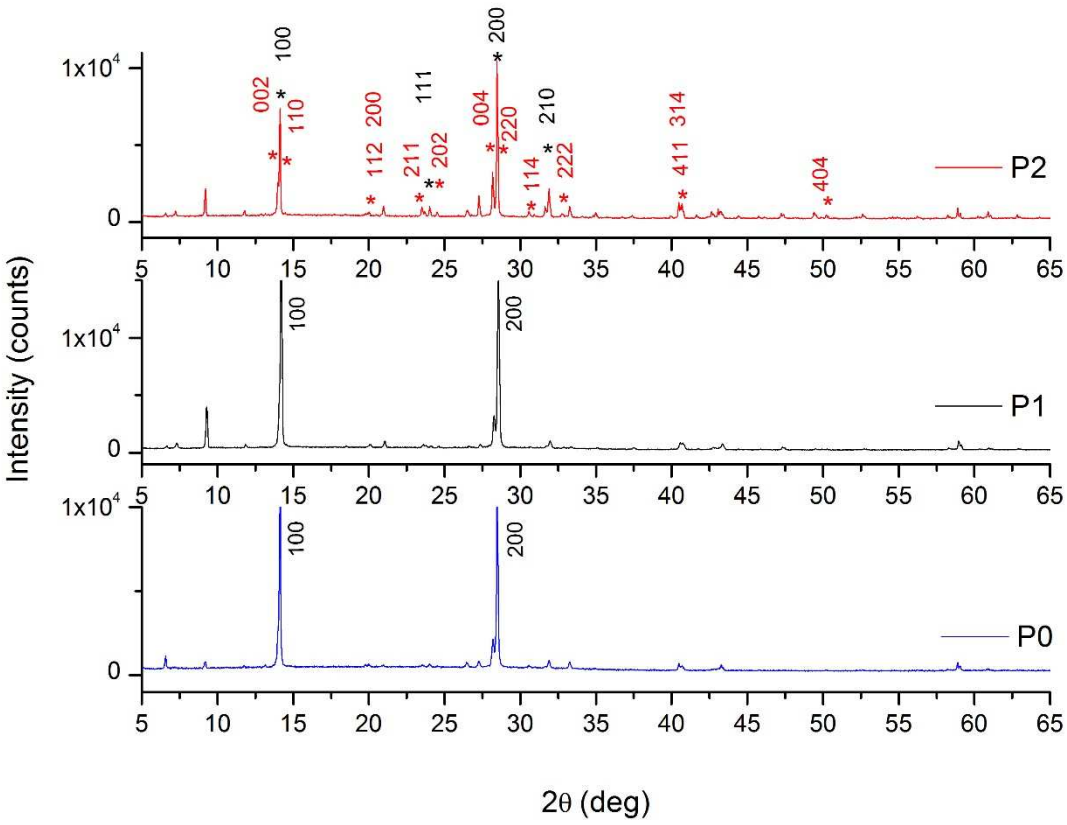

Figure-3. XRD patterns for $CH_3NH_3PbI_3$ thin films deposited with different spin speeds on glass substrates

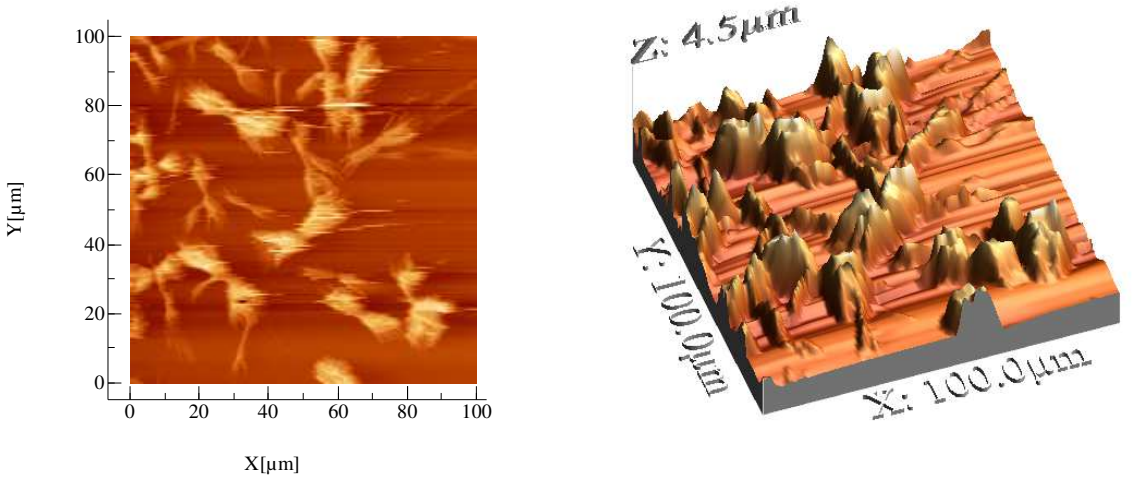

P0 RMS = 0.537µm, RA =0.389µm

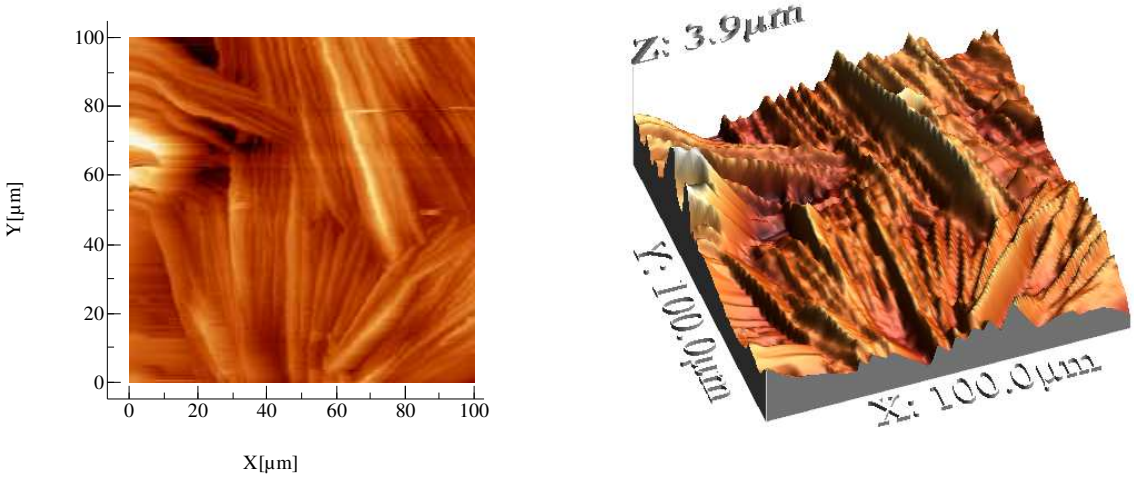

P1 RMS = 0.469µm, RA =0.349µm

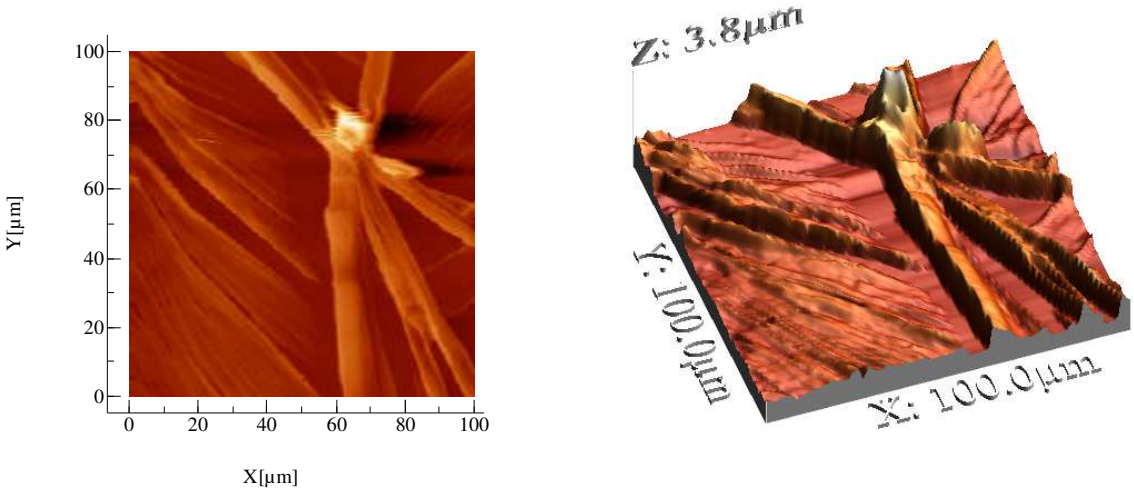

P2 RMS = 0.369µm, RA =0.270µm

Figure-4. 2D and 3D AFM images for $CH_3NH_3PbI_3$ thin films deposited with different spin speeds on glass substrates.

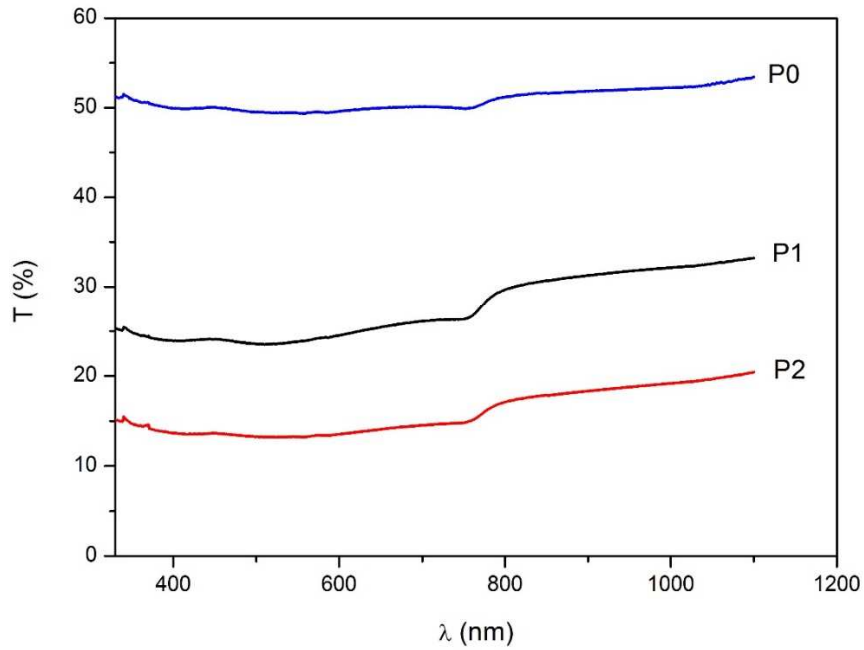

Figure-5. Transmission coefficients for $CH_3NH_3PbI_3$ thin films deposited with different spin speeds on glass substrates

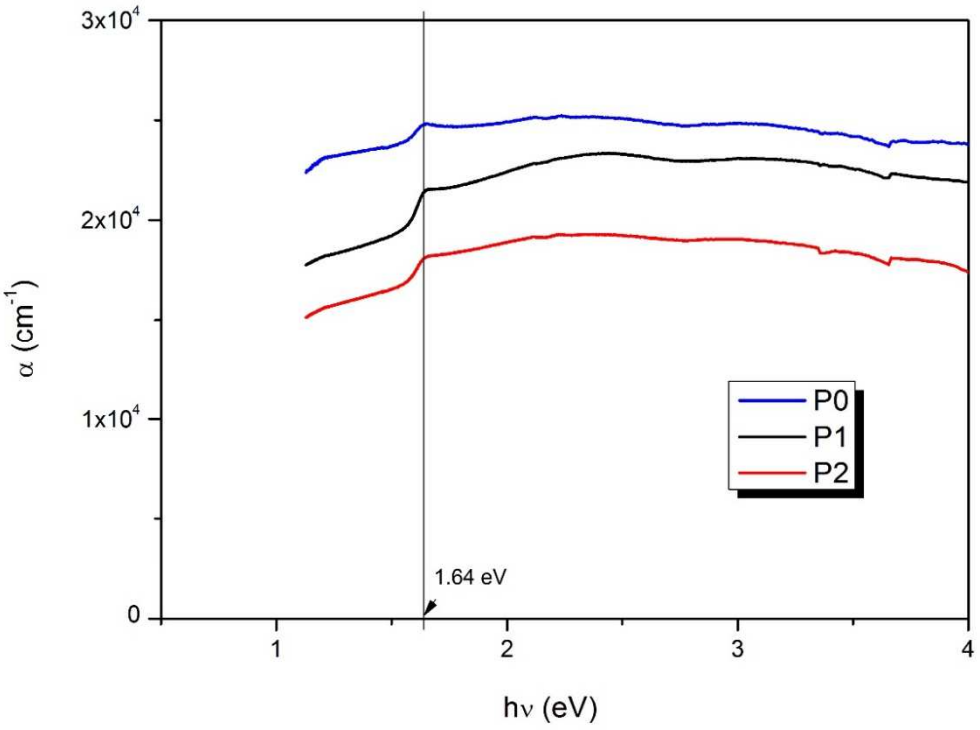

Figure-6. The absorption coefficient vs. photon energy for films $CH_3NH_3PbI_3$ thin films deposited on glass substrates with different rotations speeds

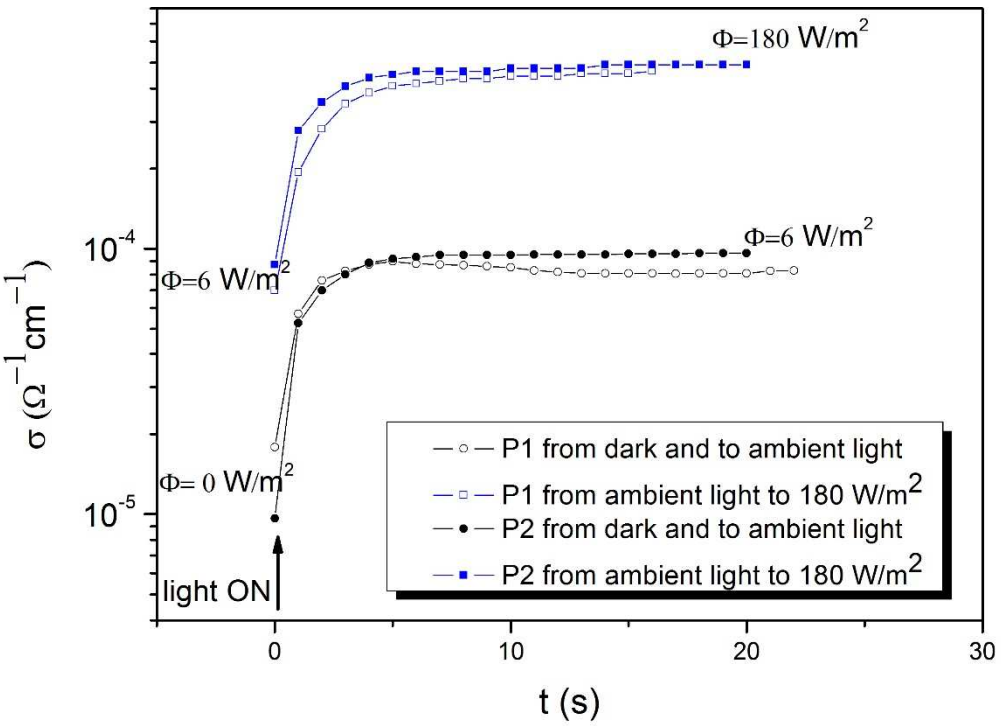

Figure-7. The variation of the electrical conductivity in function of time for the samples P1 and P2, after the exposure of the samples from dark conditions (0W/m^2) to ambient light (6W/m^2), and then from ambient light condition (6W/m^2) to an exposure under a white light source (180W/m^2).

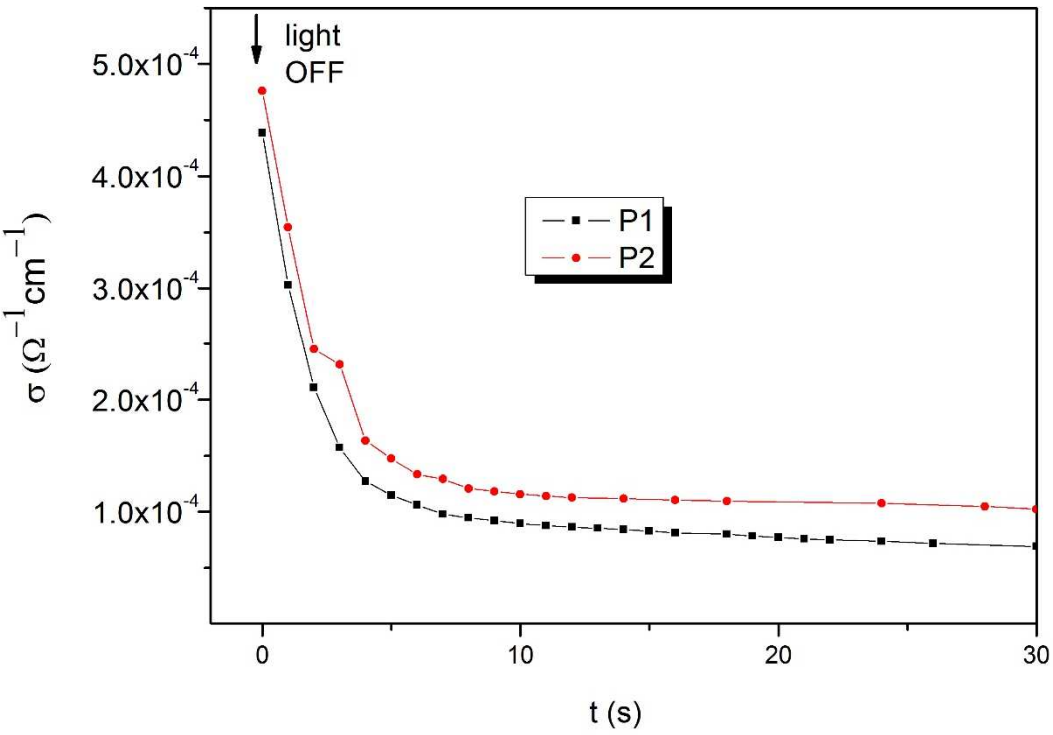

Figure-8. The electrical conductivity variation in function of time after the irradiation with a white light source (180W/m^2), to ambient light conditions (6W/m^2).

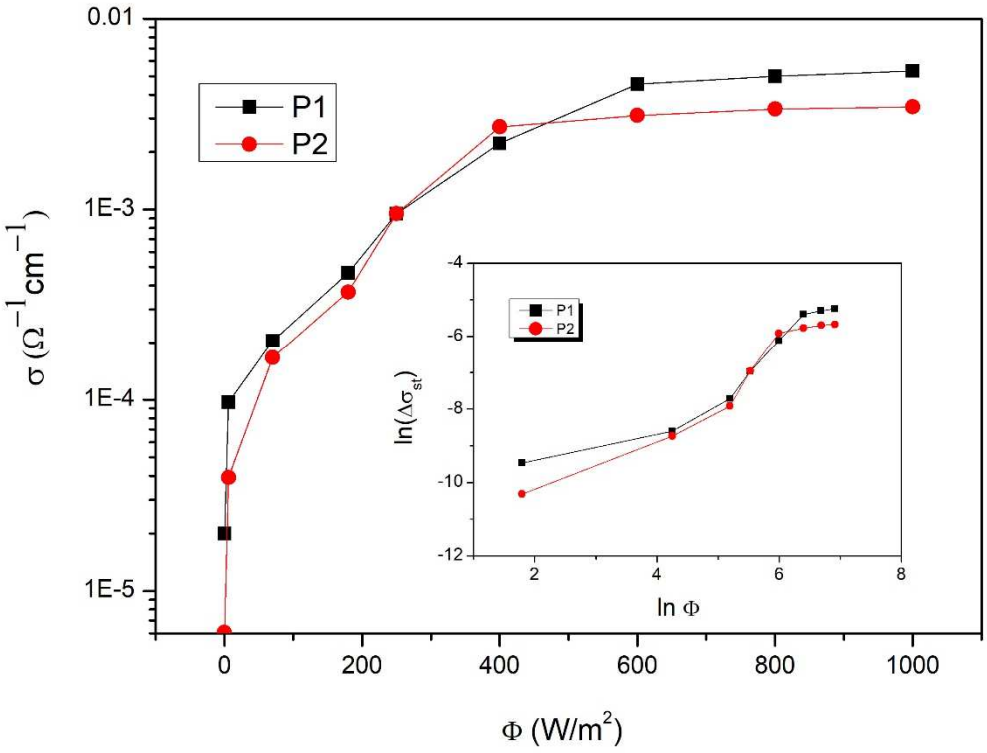

Figure-9. The variation of the electrical conductivity in function of light intensity irradiation after the saturation regime is attaint (after more than 60 seconds) for two samples deposited with different spin speeds, having a different thickness. The inset gives the dependencies of the photoconductivity logarithm in function of the light intensity logarithm.

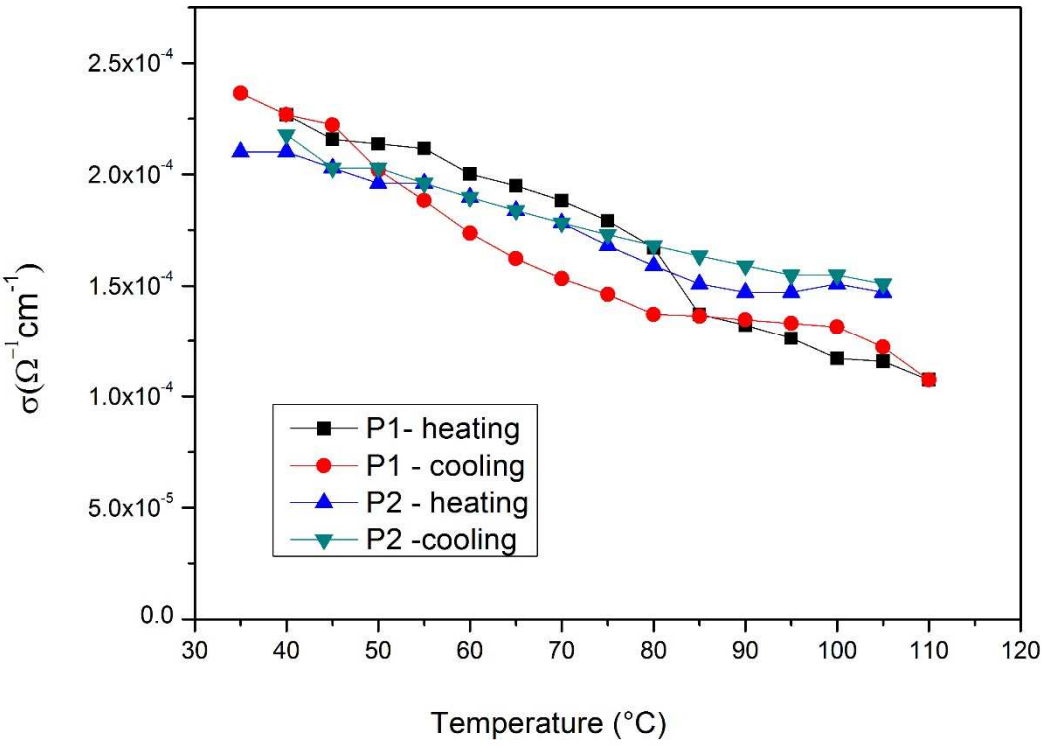

Figure-10. The variation of the electrical conductivity in function of temperature measured under illumination (70W/m^2) with a white light source during one cycle of heating and cooling for two samples deposited with different spin speeds, having a different thickness.

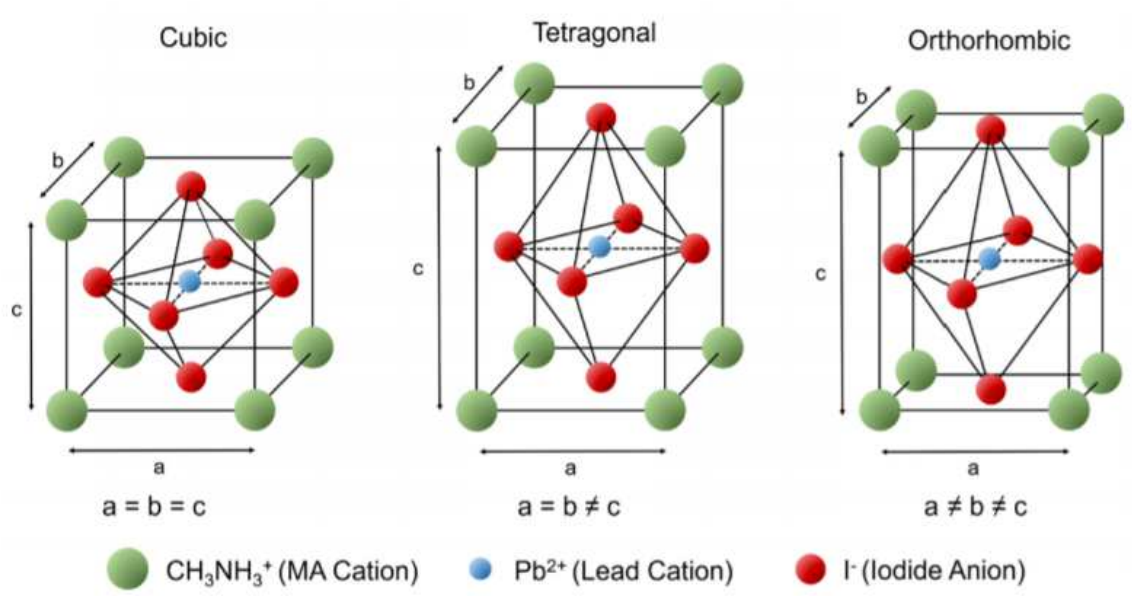

Figure-11. The unit cells for cubic, tetragonal and orthorhombic phases of $CH_3NH_3PbI_3$ perovskite.

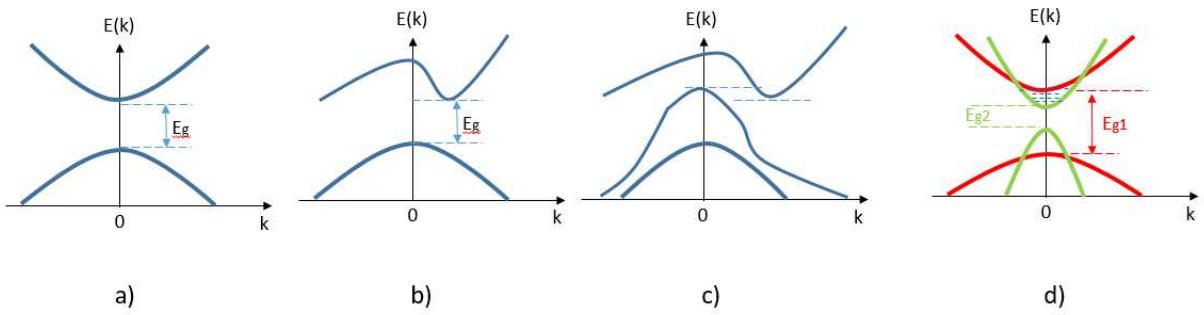

Figure-12. Semiconductor band structures: a) aligned bands (direct band gap) b) not-aligned bands (indirect band gap) c) overlapped bands d) multiband model.

Graphical Abstract

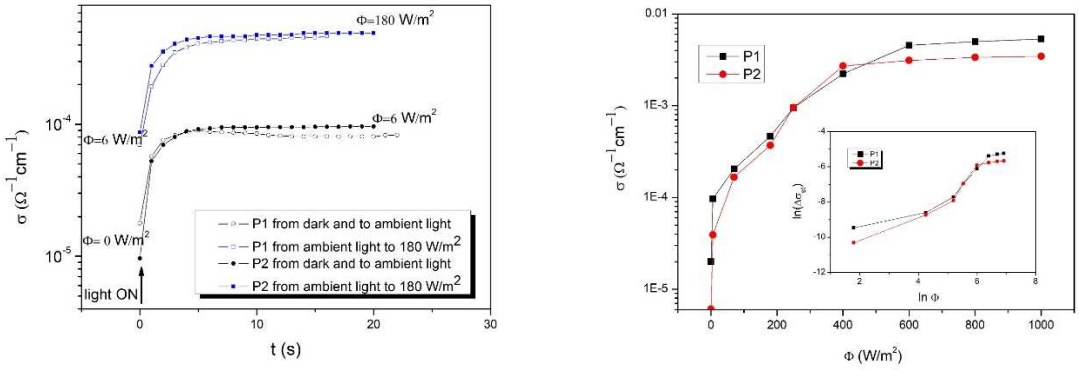

a) b)

Fig. Response of perovskite thin films electrical conductivity to light variation

a) in function of time b) in function of light intensity